Radical pathways in the thermal decomposition of pyridine and diazines: a laser pyrolysis and semi-empirical study

Nathan R. Hore and Douglas K. Russell *

Department of Chemistry, University of Auckland, Private Bag 92019, New Zealand

The mechanisms of thermal decomposition of pyridine and the three isomeric diazines have been investigated by IR laser pyrolysis in conjunction with stable end-product analysis by FTIR, NMR and GC–MS, and radical detection by EPR spectroscopy. Calculations at semi-empirical and *ab initio* levels have provided confirmation of potential reaction pathways. For pyridine, reaction is initiated by formation of pyridyl radicals, as indicated by extensive isotope exchange with added deuterium. Experiments with bromopyridines show that open chain radicals arising from ring opening of 2-pyridyl and 3-pyridyl radicals each lead to stable gaseous products, while 4-pyridyl radicals produce solid deposits, and may be the principal agents in soot formation. The evidence suggests that 1,2-diazine decomposes *via* a molecular route leading to stoichiometric production of HCN and C_2H_2, while 1,3- and 1,4-diazine follow a pattern of H loss and ring radical opening analogous to that of pyridine.

Introduction

The mechanism of the pyrolysis and combustion of azines, particularly of pyridine and the three isomeric diazines, is of considerable significance from both practical and fundamental perspectives. On the one hand, these compounds make a substantial contribution to the global anthropogenic NO_x budget through the combustion of solid and liquid fuels of biological origin, and they have also been implicated in the formation of soot in the combustion of nitrogen-rich fuels.[1,2] In addition, the elucidation of the relative significance of intramolecular and radical chain processes in aromatic systems is a stringent test of experimental and theoretical methodologies.[3]

The earliest investigation of azine pyrolysis appears to be that of Roth,[4] who noted hydrogen cyanide and bipyridyls as the major products of pyrolysis of pyridine. The generation of bipyridyls (largely the 2,2′ isomer) was confirmed by other early workers, who also detected hydrogen and acetylene at higher temperatures.[5,6] In 1962, Hurd and Simon[7] detected acetonitrile (cyanomethane) and acrylonitrile (cyanoethene) among the nitrogenous products of pyrolysis of pyridine in a flow system at 1100–1200 K. A detailed kinetic study by Axworthy *et al.*[8] determined a first-order rate constant of $3.8 \times 10^{12}\exp(-290\ \text{kJ mol}^{-1}/RT)\ \text{s}^{-1}$ for the decomposition of pyridine, parameters broadly confirmed by Houser *et al.*[9] and Kern *et al.*[10] However, more recent work,[11,12] carried out in shock tubes at low pressure, indicates much higher activation energies near 400 kJ mol^{-1}. A particularly detailed study has been reported by Mackie and co-workers,[12,13] who fitted the temperature dependence of the observed pyridine loss and end product distribution to a 58 step reaction scheme; these workers also identified acetylene and cyanoacetylene as significant end-products at high temperatures. The most extensive experimental investigations of diazine pyrolysis have been reported by the same group,[14,15] who have also explored the aspects of the energetics of radical and potential intramolecular routes through high level *ab initio* studies.[3]

Free radicals feature as key intermediates in all the reaction schemes proposed by Mackie *et al.* and earlier workers,[3,12–15] but end-product analysis alone provides little direct evidence for the relative significance of radical production and loss processes. We have shown elsewhere that the technique of Infrared Laser Powered Homogeneous Pyrolysis (IR LPHP) of appropriate systems, supported by a range of analytical methods and calculations, can provide detailed mechanistic information on pyrolysis pathways in many systems.[16] In the present work, we report a detailed investigation of the role of radical intermediates in the pyrolysis of pyridine, pyridazine (1,2-diazine), pyrimidine (1,3-diazine) and pyrazine (1,4-diazine) by the methods established earlier.

Experimental methods and calculations

All compounds used in this study were 'AR' grade (Acros or Lancaster); these and SF_6 (BOC) were purified prior to use by repeated freeze–thaw–pump cycles. All samples were handled on a rigorously pre-conditioned vacuum line fitted with greaseless Youngs taps. The compounds 4-bromopyridine and 4-chloropyridine are somewhat unstable at room temperature when free of hydrochloric acid,[17] and were therefore prepared as needed by extraction from their stable hydrochloride salts into an organic solvent. The solvent was partially removed by means of a rotary evaporator at room temperature before transfer to a vacuum line for removal of the remaining solvent at −70 °C. This resulted in the pure compound which was stable at this temperature until required.

All experimental pyrolysis studies were carried out using the method of IR LPHP. This technique has been described in detail elsewhere[18–20] and therefore only a brief description is given here. Pyrolysis is carried out in a cylindrical Pyrex cell (length 10 cm, diameter 3.8 cm) fitted with ZnSe windows. The cell is filled with a few Torr (1 Torr = 133.3 Pa) of the vapour under study and *ca.* 10 Torr of SF_6. In cases where sample vapour pressure is insufficient for transfer in the vapour phase, a small amount of liquid or solid is introduced directly into the pyrolysis cell, and volatile impurities removed *in situ* by freeze–thaw–pump cycles. The contents of the cell are then exposed to the output of a free running CW CO_2 laser at 10.6 μm at a power level depending on the temperature required for periods leading to decomposition of up to 25%. As shown elsewhere,[18–20] the SF_6 strongly absorbs the laser radiation, which is then converted to heat *via* very rapid inter- and intramolecular relaxation. The low thermal conductivity of the SF_6 ensures that this produces a strongly inhomogeneous temperature profile, in which the centre of the cell may reach temperatures as high as 1500 K while the cell walls remain at room temperature.

The IR LPHP technique has a number of well-documented advantages. The first of these is that pyrolysis is initiated directly in the gas phase, entirely eliminating the complications frequently introduced by competing surface reactions; this is of

Table 1 IR features used in the determination of reactants and selected products of IR LPHP of azines

Molecule	Feature/cm^{-1}	Literature/cm^{-1}
HCN	712 (PQR), HCN bend	712[a]
HCCCN	663 (PQR), CCH bend	663[b]
C_2H_2	729 (PQR), CCH bend	729[a]
C_5H_5N	700 (PQR)	700[c]
2-BrC_5H_4N	758 (PQR)	760[c]
3-BrC_5H_4N	700 (PQR)	700[c]
4-BrC_5H_4N	677 (PQR)	680[c]
4-ClC_5H_4N	809 (PQR)	810[c]
1,2-$N_2C_4H_4$	756 (PQR)	760[c]
1,3-$N_2C_4H_4$	718 (PQR)	720[c]
1,4-$N_2C_4H_4$	784 (PQR)	790[c]

[a] G. Herzberg, *Infrared and Raman Spectra of Polyatomic Molecules*, Van Nostrand, New York, 1945. [b] Ref. 12. [c] D. R. Lide and G. W. A. Milne, *Handbook of Data on Organic Compounds*, 3rd edn., CRC Press, London, 1984.

considerable value in systems where free radicals are implicated, since their role is likely to be enhanced by surface processes. The second is that less volatile primary pyrolysis products are rapidly ejected into cool regions of the cell, where they are not subject to further reaction. In favourable cases, these products may be accumulated for further reaction or analysis. On the other hand, the temperature of the pyrolysis is neither well defined nor easily determined, so that comparison with more conventional methods of pyrolysis is not straightforward. Furthermore, the effective temperature is in part determined by the conductivity of the gaseous cell contents, and hence may vary over the course of the reaction. Nevertheless, an initial effective temperature may be estimated from the rate of disappearance of a compound with known (and comparable) kinetic parameters. In the present experiments, the effective first-order rate constant for the low temperature decomposition of pyridine reported by Ikeda and Mackie[12] provided an estimate of between 1100 and 1150 K for all experiments involving unsubstituted azines, and substantially lower (*ca.* 1000 K) for halogenated compounds.

All stable products other than H_2 or N_2 (see below) were identified by either FTIR spectroscopy or GC–MS. IR spectra were recorded using a Digilab FTS60 FTIR spectrometer at a resolution of 1 cm^{-1}. A list of the distinctive and isolated features used for FTIR spectroscopy is given in Table 1. Where appropriate, product distributions were quantified with the aid of the MOLSPEC software package,[21] based on the 1986 edition of the HITRAN database.[22] All FTIR spectra were recorded directly (either as vapour or as deposit on the windows) in the 10 cm long pyrolysis cell described above fitted with ZnSe windows. Although this material has a relatively high cut off at the low frequency end (*ca.* 500 cm^{-1}), for our LPHP work it possesses several advantages in that it has a lower absorption of the CO_2 IR laser radiation at 10.6 μm, lower thermal expansion and higher thermal conductivity than materials such as NaCl or KCl. It is also less hygroscopic than these materials, a factor that can be crucial when dealing with moisture sensitive compounds. The more conventional materials are also prone to thermal stress and may fracture during pyrolysis at the high laser powers employed here.[23]

GC–MS work was carried out on Hewlett Packard 5890 or 6890 gas chromatagraphs coupled with Hewlett Packard 5971 or 5973 mass selective detectors. The GC employed cross-linked methyl silicone or phenyl methyl siloxane gum capillary columns of 0.33 μm film thickness and 25 m by 0.2 mm internal diameter. Pyrolysis samples for GC–MS analysis were vacuum distilled directly from the pyrolysis cell into a small Pyrex tube fitted with a Youngs tap and a rubber septum. Samples were then extracted through the rubber septum by means of a GC–MS needle, thereby eliminating atmospheric contamination. Toluene or dichloromethane was used as the solvent for all GC–MS spectra.

Table 2 Calculated activation energies (kJ mol^{-1}) for hydrogen loss reactions

Resultant radical	AM1[a]	PM3[a]	3-21G HF[a]	(RO)MP2/DZP// (RO)HF/3-21G[b]
2-Pyridyl	426	409	352	435
3-Pyridyl	445	428	363	459
4-Pyridyl	438	423	358	451
3-Pyridazyl	443	—	—	439
4-Pyridazyl	450	—	—	453
2-Pyrimidyl	433	—	358	436
4-Pyrimidyl	431	—	354	433
5-Pyrimidyl	458	—	434	463
Pyrazyl	437	—	—	434

[a] This work. [b] Ref. 3.

^{1}H NMR spectra were recorded at 200 MHz using a Bruker AM200 FT NMR spectrometer. Samples for NMR were vacuum distilled directly from the pyrolysis cell into NMR tubes fitted with Youngs taps. [$^2H_3$]Acetonitrile was used as both solvent and internal reference for all NMR spectra.

EPR spectroscopy was carried out using a Varian E-4 EPR spectrometer. Reagents for EPR analysis were pumped through a conventional resistively heated hot-wall quartz tube by means of oil diffusion and rotary pumps at pressures of much less than 1 Torr. Pyrolysis products were condensed onto a cold finger cooled to 77 K by liquid nitrogen. The whole cold finger assembly was then removed from the line by glass-blowing and inserted into a standard wide-bore Varian cavity for the examination of EPR spectroscopy.[20] Many experiments were performed between the range of 250–700 °C; the strongest signals were provided by temperatures of *ca.* 500 °C. Radicals were usually trapped in matrices of unreacted starting material. In some experiments, adamantane was added as a matrix host in the hope that this would provide more easily interpretable resolved isotropic EPR spectra. In the event, this proved not to be the case, and adamantane matrices thus provided little advantage.

Indicative calculations of structures, energies and transition states were carried out at modest semi-empirical (AM1 or PM3) or *ab initio* (3-21G or 6-31G*) levels with the aid of either MOPAC Version 6 (ref. 24) on a RS 6000/590 IBM workstation, or the PC Spartan or Spartan Plus molecular modelling packages on a high platform PC.[25] All calculations were carried out using self-consistent field methods with either a restricted or unrestricted Hartree–Fock depending on the calculation. *Ab initio* calculations were performed with either the predetermined 3-21G split valence or 6-31G* polarisation basis sets. All structures were located by minimising the norm of the analytical energy gradient to less than 5×10^{-9} N. Transition states were located by ensuring that the hessian matrix (matrix of energy second derivatives) possessed only one negative frequency corresponding to the reaction path, verified in the case of the Spartan programmes by visualisation of the appropriate coordinate. As in earlier work,[16] calculations were benchmarked where possible against high level theoretical or experimental literature reports, and the method yielding the most reliable results for the particular class of reaction under consideration then selected. For the majority of reactions and species studied here, calculations at the AM1 semi-empirical level provided results very close to those of Jones *et al.*,[3] who reported calculations at the (RO)MP2/DZP///(RO)SCF/3-21G level (Table 2); we have therefore used AM1 calculations throughout the present work.

Observations

1. Pyridine

As described in the Introduction, the pyrolysis of pyridine has

previously been investigated using static, flow and shock-tube techniques.[4–13] However, most of the early studies were directed towards end product identification and the measurement of the overall kinetic parameters of decomposition rather than elucidation of mechanistic detail. Recently, Mackie and co-workers studied the kinetics of loss of pyridine and formation of products in a single pulse shock tube between 1300–1800 K using GC–MS and FTIR for product analysis,[12] and also carried out a detailed study of the pyrolysis of pyridine and 2-picoline in a fused silica stirred reactor[13] between 1060–1240 K. The low temperature pyrolysis, which is of greater relevance to the present work, yielded cyanoacetylene as the major nitrogen-containing product, while HCN dominated at higher temperatures; other major products were acetylene and hydrogen. Kern *et al.*[10] proposed a chain mechanism for the decomposition of pyridine initiated through ring-hydrogen homolytic fission, a route generally accepted as the major initiation reaction in many aromatic systems. Thermochemical estimates of the chemistry of the resulting cyclic pyridyl radicals reported by Mackie *et al.*[12] suggested that the 2-pyridyl radical was unique in its propensity for facile cleavage. This finding was rationalised in terms of the stability of the resultant open chain cyano radical from which cyanoacetylene is subsequently produced. Several potential sources of HCN were identified in the resultant scheme; however, HCN was not identified as a primary reaction product. The major low temperature reaction mechanism proposed by Mackie *et al.* is summarised in Scheme 1.

$$C_5H_5N \longrightarrow 2\text{-, } 3\text{-, } 4\text{-}C_5H_4N^{\bullet} + H^{\bullet} \quad (1)$$

$$2\text{-}C_5H_4N^{\bullet} \longrightarrow {}^{\bullet}CH{=}CH{-}CH{=}CH{-}CN \quad (2)$$

$${}^{\bullet}CH{=}CH{-}CH{=}CHCN \longrightarrow C_2H_2 + {}^{\bullet}CH{=}CHCN \quad (3)$$

$${}^{\bullet}CH{=}CHCN \longrightarrow HCCCN + H^{\bullet} \quad (4)$$

$$H^{\bullet} + C_5H_5N \longrightarrow 2\text{-, } 3\text{-, } 4\text{-}C_5H_4N^{\bullet} + H_2 \quad (5)$$

Scheme 1 Principal low temperature reactions in the pyrolysis of pyridine

It has also been suggested that 3- and 4-pyridyl radicals may eliminate HCN in molecular processes,[12] but the chemistry of these species remains uncertain. As indicated above, the principal aim of the present work is the further clarification of the involvement of all possible pyridyl radicals.

Initial investigations using FTIR detection confirmed that low temperature (1100–1150 K) IR LPHP of pyridine produced cyanoacetylene, acetylene and presumably hydrogen as the major products (hydrogen is not detected by any of our techniques, and its formation is therefore inferred from the results of earlier workers), together with HCN. Acrylonitrile (cyanoethene), vinylacetylene (but-1-en-3-yne) and diacetylene (buta-1,3-diyne) were also detected in smaller quantities using GC/MS. The distribution of these products corresponds well with that determined at low temperature by Mackie *et al.*,[12,13] confirming the homogeneous nature of both methods. The significant portions of FTIR spectra of pyridine ($+SF_6$) before and after pyrolysis are presented in Fig. 1.

Semi-empirical and *ab initio* calculations performed at a range of levels of sophistication (Table 2) found that the activation energies of reactions leading to the production of the three pyridyl radicals coincide within 20 kJ mol^{-1}, a range which is likely to have little effect at the temperatures employed in the present study. All three radicals are therefore expected to play a part in the overall IR LPHP process, and subsequent investigations were directed towards disentangling these contributions.

Thermochemical arguments, supported by reactions rates estimated in the detailed kinetic study,[12] suggest that reaction of pyridyl radicals with excess hydrogen is likely to be rapid; the

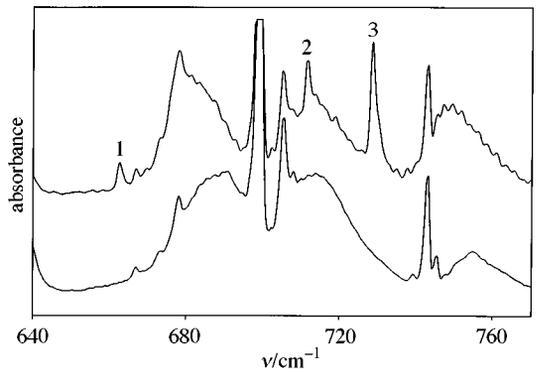

Fig. 1 FTIR spectrum (640–770 cm^{-1}) of SF_6 + pyridine before (lower) and after (upper) IR LPHP. In this and all other IR spectra, 1 = HCCCN, 2 = HCN, 3 = C_2H_2, and unassigned features = SF_6 or starting material as vapour or as deposits on the cell windows. The occasional fringing observed arises from thin films deposited on the windows.

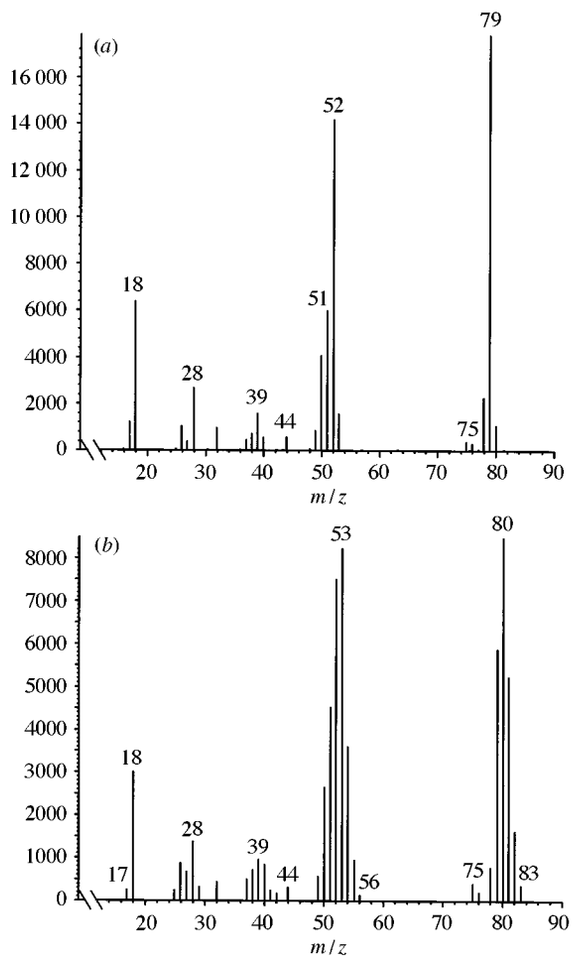

Fig. 2 Mass spectrum of [$^2H_5$]-pyridine (*a*) before and (*b*) after laser co-pyrolysis with D_2

copyrolysis of isotopomers of pyridine and hydrogen was therefore studied in order to explore the production and fate of such radicals. Fig. 2 shows mass spectra of [$^1H_5$]-pyridine and of residual pyridine after laser copyrolysis with D_2 (D_2 : pyridine = 1 : 1). Such spectra clearly revealed close to statistical isotope exchange (*ca.* 35% in Fig. 2) in isotopomers up to [$^2H_4$]-pyridine (*m*/*z* 83), but much lower levels of [$^2H_5$]-pyridine (*m*/*z* 84), even in experiments with higher D_2 : pyridine ratios. Somewhat increased yields of acrylonitrile relative to cyanoacetylene, and of vinylacetylene relative to diacetylene, were also found for the copyrolysis reactions in which either H_2 or D_2 had been added, while HCN yields remained almost constant.

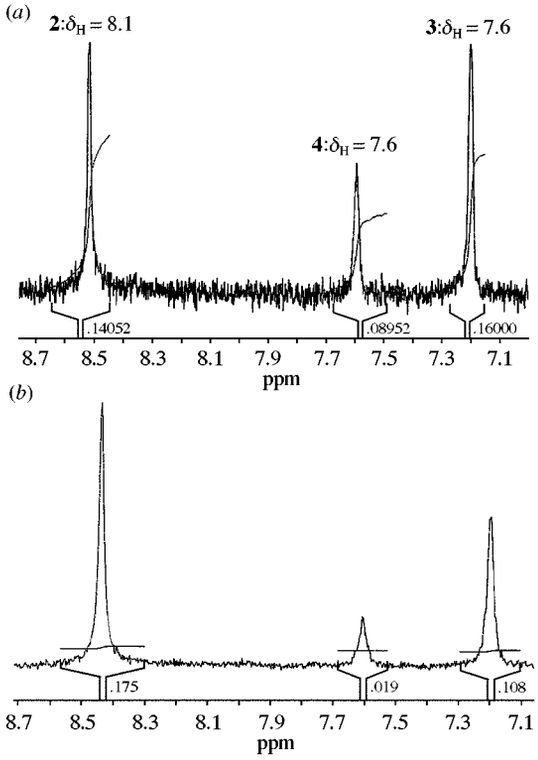

Fig. 3 ^{1}H NMR spectrum of [$^2H_5$]-pyridine (*a*) before and (*b*) after laser co-pyrolysis with H_2

Clarification of this finding was sought through ^{1}H NMR spectroscopy of the products of copyrolysis of [$^2H_5$]-pyridine with H_2. Fig. 3 shows the pre- and post-copyrolysis ^{1}H NMR spectra of [$^2H_5$]-pyridine at low levels of exchange. The ratio of the residual proton impurity in [$^2H_5$]-pyridine before pyrolysis is close to the statistical 2:2:1 for the 2, 3 and 4 positions. After pyrolysis, the level of protonation at the 2 and 3 positions increased substantially in the approximate proportions of 2:1, while that at the 4 position was little affected.

2. Bromopyridines

The reports of Mackie *et al.*,[12,13] together with results for pyridine described above, suggest that the fates of the 2-, 3- and 4-pyridyl radicals differ substantially, and that it would be advantageous to study their reactions in isolation in order to clarify their decomposition chemistry. For this purpose, 2-, 3- and 4-bromopyridines proved invaluable, allowing clean generation of the respective pyridyl radicals; the substantially weaker C–Br bond provides a low energy route to the corresponding pyridyl radical, thereby permitting a considerably lower pyrolysis temperature (≈1000 K) and reducing complicating secondary reactions. The relatively unreactive bromine atoms played no detectable further part in the system, presumably eventually recombining to form the molecular bromine visible in the pyrolysis cell.

FTIR spectra of 2- and 3-bromopyridine (+SF_6) after laser pyrolysis at *ca.* 1000 K each revealed the major products obtained from the pyrolysis of pyridine, with more HCN and less cyanoacetylene in the case of 3-bromopyridine. However, for both the production of cyanoacetylene is substantially increased, and that of HCN decreased, relative to that from pyridine. The observation that 3-bromopyridine undergoes decomposition to the same end products as 2-bromopyridine is significant in that it confirms that the 3-pyridyl radical also plays an important part in the decomposition chemistry of the pyridine. GC–MS examination of the products of co-pyrolysis of 2-bromopyridine with D_2 at low laser powers (sufficient to initiate C–Br homolysis, but not to generate HCN) revealed the formation of singly deuteriated pyridine only. On the other hand, 4-bromopyridine behaved quite differently in that no gas phase products at all were detectable after pyrolysis. Instead, very substantial solid deposits were evident on the windows and walls on the pyrolysis cell. The same result was observed with the 4-chloro compound, which is somewhat more stable at room temperature.

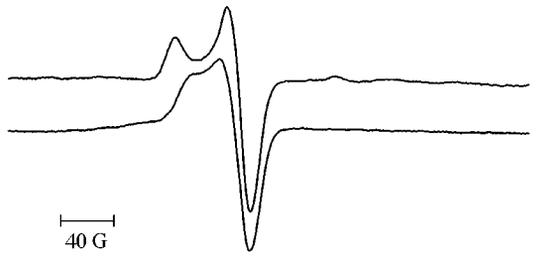

Fig. 4 EPR spectra of products of pyrolysis of CH_2Cl_2 (above) and pyridine (below)

Finally, the role of radicals in the decomposition of pyridine was investigated by EPR spectroscopy. Pyridine and all brominated compounds produced very similar and characteristic spectra, consisting of a broad anisotropic signal centred at $g = 2.0025$ with little discernible fine structure; this *g*-value is identical to that of the standard pitch sample, which consists of charred organic compounds dispersed in KCl. This signal is very similar to that produced in the pyrolysis of many organic compounds, and has been ascribed to surface 'dangling bonds' in amorphous carbon and carbides; minor variations, for example in the observed degree of anisotropy, arise from the extent of aggregation of carbon, although *g*-values are all very similar.[26] For example, very strong such spectra are produced by the pyrolysis of dichloromethane, which is known to undergo a facile double 1,1 elimination[27] of HCl; $CH_2Cl_2 \longrightarrow C + 2HCl$. Consequently, the strength of this signal might be interpreted as a direct measure of the sooting tendency of the compounds studied here. Fig. 4 shows an example of such an EPR spectrum resulting from the pyrolysis of pyridine, together with that from dichloromethane. Of major significance here is the relative intensity of the radical signals; while small differences resulted from inevitable variations in temperatures and flow rates, the signals obtained from the 4-bromopyridine were always at least two orders of magnitude larger than those obtained from the other compounds.

3. Pyridazine

Apart from some consideration in the theoretical study of Jones *et al.*,[3] there appears to have been no previous work on the thermal decomposition of pyridazine (1,2-diazine). This may arise from the apparent predictability of the course of its pyrolysis, namely the intramolecular elimination of N_2 and $2C_2H_2$; there is, of course, a second feasible intramolecular route yielding 2HCN and C_2H_2. The former is favoured both on thermochemical grounds[28] ($\Delta_f H = +453$ kJ mol^{-1} for $N_2 + 2C_2H_2$, +489 kJ mol^{-1} for 2HCN + C_2H_2) and by calculation at modest levels. As noted elsewhere,[3] the absolute reliability of low-level calculations for this kind of reaction is extremely limited, since dynamic electron correlation effects are likely to be very significant; however, relative values are of some interest.

Fig. 5 shows FTIR spectra of pyridazine before and after pyrolysis. Both in these spectra, and using all other techniques, the only detectable pyrolysis products were HCN and C_2H_2; in particular, there was no trace of cyanoacetylene or C_4 species.

Simulations of the spectrum of Fig. 5 indicated a ratio of 2:1 for HCN:C_2H_2, closely matching that of the thermodynamically less favoured molecular elimination route.

4. Pyrimidine

The pyrolysis of pyrimidine has previously been investigated by Doughty and Mackie[14] in single-pulse shock tubes between

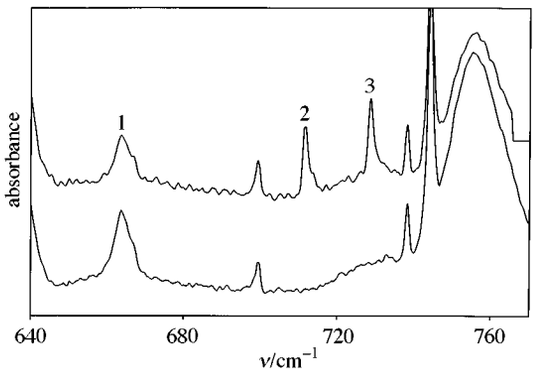

Fig. 5 FTIR spectrum of SF_6 + pyridazine before (lower) and after (upper) IR LPHP

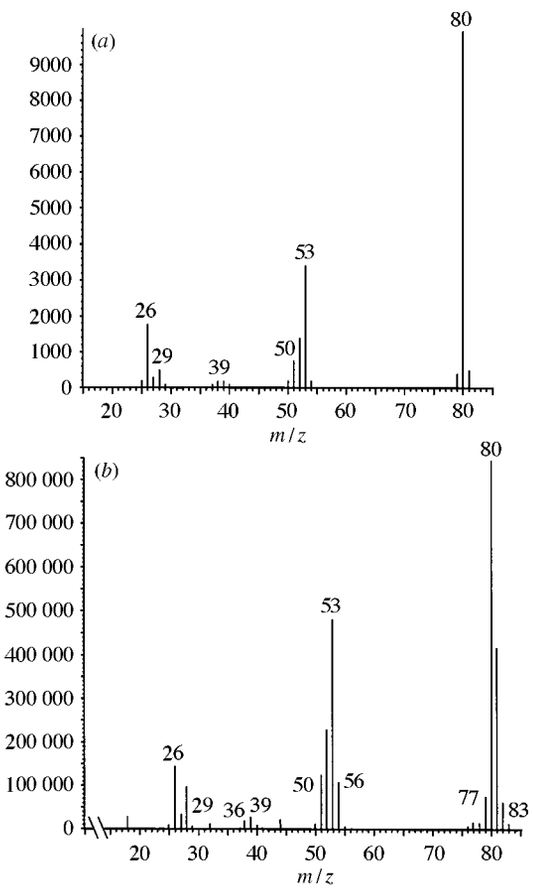

Fig. 6 Mass spectrum of pyrimidine (*a*) before and (*b*) after laser copyrolysis with D_2

1200–1850 K; at low temperatures, pyrolysis yielded HCN, cyanoacetylene and acrylonitrile as major products, with C_2H_2 in smaller quantities. FTIR and GC–MS analysis of products of laser pyrolysis of pyrimidine concurred entirely with these findings of Doughty and Mackie.

As with pyridine, the initiation reaction for pyrimidine is expected to involve ring-hydrogen homolytic fission, with the resulting pyrimidyl radicals ring-opening and then undergoing further reaction. Thermochemical estimates indicated that the enthalpy of formation of the 2-pyrimidyl radical is the lowest, with 4-pyrimidyl some 30 kJ mol^{-1} higher and 5-pyrimidyl a further 35 kJ mol^{-1} higher still.[14] The pyrolysis mechanism proposed by Doughty and Mackie therefore centred around the ring-opening of 2- and 4-pyrimidyl radicals to open chain cyano radicals, which then decompose to stable products. On the other hand, both our own calculations (at levels shown above to be reliable to ~15 kJ mol^{-1} in the case of pyridine) and

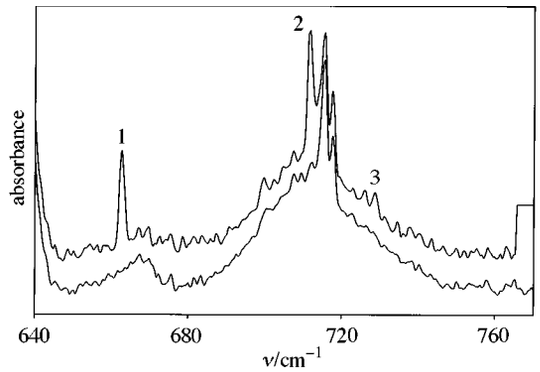

Fig. 7 FTIR spectrum of SF_6 + 5-bromopyrimidine before (lower) and after (upper) IR LPHP

subsequent investigations by Jones *et al.*[3] suggest that activation energies for hydrogen loss from all three positions are comparable (Table 2). The approaches successfully exploited for pyridine were therefore extended to pyrimidine.

Pyrimidine was copyrolysed with D_2 in order to investigate the extent of deuteriation and hence the involvement of radicals. Mass spectra, of which Fig. 6 is typical, showed that copyrolysis of pyrimidine with D_2 results in extensive and essentially statistical deuteriation at up to three of the four possible sites, a result entirely analogous with the pyridine system.

The 5-pyrimidyl radical differs from 2- and 4-pyrimidyl radicals in that it cannot undergo facile ring opening to a cyano radical. However, the open chain radical arising from ring opening of 5-pyrimidyl is N-terminated; it is therefore analogous to the open-chain radical produced in the decomposition of pyridine or 3-bromopyridine, which we have shown above to decompose to stable end products. Therefore, a clean route into the 5-pyrimidyl radical was sought; by analogy with pyridine, the chosen source was 5-bromopyrimidine. Fig. 7 shows the FTIR spectra of 5-bromopyrimidine before and after pyrolysis.

As is evident in Fig. 7, only HCN and cyanoacetylene were detected as significant products; no trace of acetylene was found.

5. Pyrazine

Pyrazine has also previously been investigated by Doughty *et al.*[15] in a single-pulse shock tube between 1200–1480 K. C_2H_2 and HCN were identified as major products, with smaller amounts of cyanoacetylene and acrylonitrile. To complete the present study, pyrazine was also studied using the IR LPHP technique, although there is no ambiguity over the identity of the primary radical intermediate. FTIR spectra of pyrazine after laser pyrolysis revealed C_2H_2, HCN and cyanoacetylene, concurring entirely with the products observed by Doughty *et al.* Doughty *et al.* also reported the isomerisation of pyrazine to pyrimidine. However, no experimental evidence for the formation of pyrimidine was found at the slightly lower temperatures employed in the present study.

Discussion and conclusions

The experimental observations reported here support those of earlier studies, and provide substantial mechanistic insight. As shown in Table 2, calculations at the AM1 semi-empirical level have been shown to provide estimates reliable to 25 kJ mol^{-1} for the heats of formation of the majority of species involved in likely pathways. Results are therefore discussed in the context of the results of calculations at this level presented in Table 3. In addition to estimates of enthalpies of formation for starting materials and cyclic radicals resulting from initial H-atom loss, calculations for the possible terminal radicals arising from

Table 3 AM1 calculated heats of formation (kJ mol^{-1}) of key species in azine pyrolysis

Compound	$\Delta_f H$	Cyclic radical	$\Delta_f H$	Open chain radical	$\Delta_f H$	Initial products	$\Delta_f H$
Pyridine	134	2-pyridyl	342	N≡C–CH=CH–CH=CH$^{\bullet}$	435	N≡C–CH=CH$^{\bullet}$ + C_2H_2	611
				HC≡C–N=CH–CH=CH$^{\bullet}$	575	HC≡C–N=CH$^{\bullet}$ + C_2H_2	707
		3-pyridyl	361	HC≡C–CH=CH–CH=N$^{\bullet}$	506	HC≡C–CH=CH$^{\bullet}$ + HCN	604
				HC≡C–CH=N–CH=CH$^{\bullet}$	579	HC≡C–CH=N$^{\bullet}$ + C_2H_2	687
		4-pyridyl	354	HC≡C–CH=CH–N=CH$^{\bullet}$	522	HC≡C–CH=CH$^{\bullet}$ + HCN	604
Pyridazine	231	3-pyridazyl	456	N≡C–CH=CH–CH=N$^{\bullet}$	417	N≡C–CH=CH$^{\bullet}$ + HCN	511
				HC≡C–N=N–CH=CH$^{\bullet}$	675	HC≡C–N=N$^{\bullet}$ + C_2H_2	685
		4-pyridazyl	463	HC≡C–CH=CH–N=N$^{\bullet}$	489	HC≡C–CH=CH$^{\bullet}$ + N_2	523
				HC≡C–CH=N–N=CH$^{\bullet}$	617	HC≡C–CH=N$^{\bullet}$ + HCN	587
Pyrimidine	184	2-pyrimidyl	399	N≡C–N=CH–CH=CH$^{\bullet}$	487	N≡C–N=CH$^{\bullet}$ + C_2H_2	624
		4-pyrimidyl	398	N≡C–CH=CH–N=CH$^{\bullet}$	429	N≡C–CH=CH$^{\bullet}$ + HCN	511
				HC≡C–N=CH–N–CH$^{\bullet}$	566	HC≡C–N=CH$^{\bullet}$ + HCN	609
		5-pyrimidyl	425	HC≡C–CH=N–CH=N$^{\bullet}$	562	HC≡C–CH=N$^{\bullet}$ + HCN	587
Pyrazine	185	pyrazyl	404	HC≡C–N=CH–CH=N$^{\bullet}$	554	HC≡C–N=CH$^{\bullet}$ + HCN	609
				N≡C–CH=N–CH=CH$^{\bullet}$	488	N≡C–CH=N$^{\bullet}$ + C_2H_2	600

ring opening of cyclic radicals, and also those resulting from subsequent terminal loss of the stable N_2, HCN or C_2H_2, are reported. With the exception of pyridazine (see below), the homolytic nature of initiation of decomposition of all compounds is confirmed both by the isotope exchange studies and the results using halogenated compounds. This is consistent with the calculations presented in both Tables 2 and 3.

For pyridine, Scheme 2 shows the dominant pathways suggested by the calculations reported in Table 3. The GC–MS and ^{1}H NMR results indicate that 2- and 3-pyridyl radicals are sufficiently long-lived to initiate exchange reactions with added hydrogen, but that 4-pyridyl radicals are not. The absence of dideuteriopyridine in the co-pyrolysis of 2-bromopyridine and D_2 indicates that exchange proceeds *via* simple abstraction ($^{\bullet}C_5H_4N + D_2 \longrightarrow {}^{\bullet}C_5H_4DN + D^{\bullet}$, *etc.*) rather than the alternative molecular addition and subsequent atom loss ($^{\bullet}C_5H_4N + D_2 \longrightarrow {}^{\bullet}C_5H_4D_2N \longrightarrow C_5H_4DN + D^{\bullet}$ or $C_5H_3D_2N + H^{\bullet}$, *etc.*). The bromopyridine results demonstrate that 2- and 3-pyridyl radicals yield identical products through two routes, with production of cyanoacetylene and acetylene dominating in the former case, and HCN and diacetylene in the latter. The lower temperature in the bromopyridine experiments also reduces the extent of secondary reaction, as expected. The 4-pyridyl radical does not apparently lead to small stable molecules through the same kind of process; instead, it leads to the formation of carbonaceous deposits, and may therefore be uniquely implicated in the formation of soot in pyridine combustion.

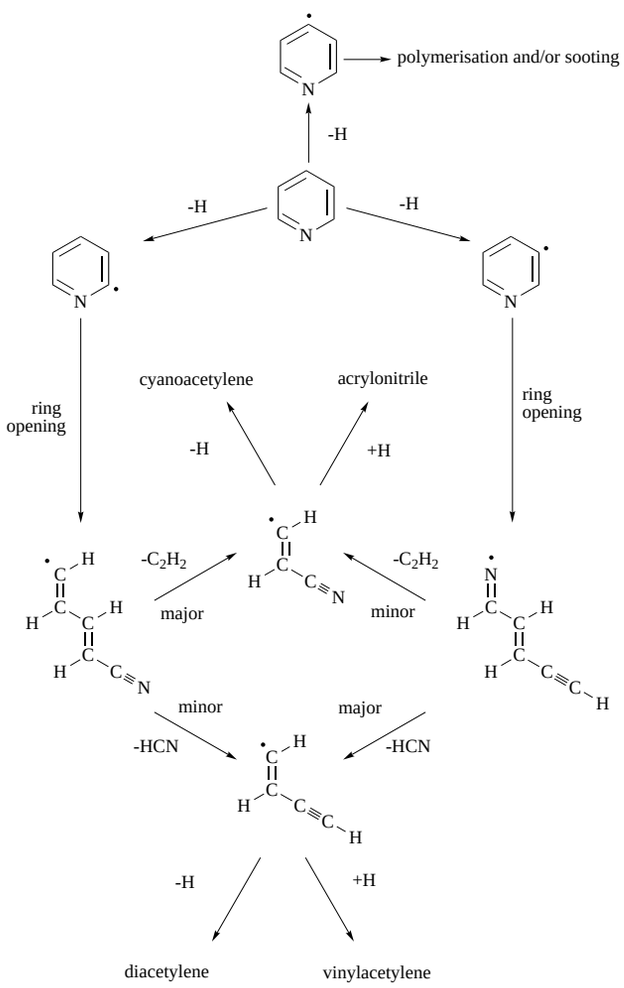

Scheme 2 Full low temperature pyridine pyrolysis scheme

The clear involvement of 3-pyridyl radicals in the formation of gas phase products is unexpected in the light of the thermochemical estimates of the heat of formation of open chain radicals.[12] However, those were based on group additivity arguments,[29] and there is considerable uncertainty within this scheme for the =N$^{\bullet}$ group. On the other hand, AM1 calculations (Table 3) for terminal radicals arising from ring opening of pyridyl radicals indicate that $\Delta_f H$ for HC≡C–CH=CH–CH=N$^{\bullet}$ (from 3-pyridyl) exceeds that for $^{\bullet}$CH=CH–CH=CH–C≡N (from 2-pyridyl) by only 70 kJ mol^{-1}. This estimate is more consistent with the role demonstrated in the present work than the group additivity value of 160 kJ mol^{-1}. What cannot be determined from these results is the stability of radicals, once formed, against intramolecular H-shifts; however, the differing relative yields of HCN and C_2H_2 suggest that they retain their integrity, at least partially.

Although H_2 is not detectable in our work, substantial amounts were observed by Mackie *et al.*;[12] these workers attributed this to abstraction of H from parent pyridine by H atoms [reaction (5) of Scheme 1], the reverse of the D-exchange reaction described above. However, the calculations reported in Table 2 suggest that such H-abstraction will be thermally neutral at best, and more probably endothermic. A more plausible source of H_2 is the H atoms lost from the immediate radical precursors to the observed end products cyanoacetylene and diacetylene, as shown in Scheme 2. Similar reactions will account for the formation of H_2 in the pyrolysis of diazines, as described below.

An analogous picture emerges for the diazines, with the exception of pyridazine. An initial H-atom loss is followed by opening of the resultant cyclic radical, loss of a stable two heavy atom species, and loss or gain of further hydrogen. For pyrimidine, the reactions of Scheme 3 show that both 4- and 5-pyrimidyl radicals result in open-chain free radicals which yield HCN and cyanoacetylene (or acrylonitrile) as the only stable end products, an expectation consistent with the results observed for 5-bromopyrimidine. On the other hand,

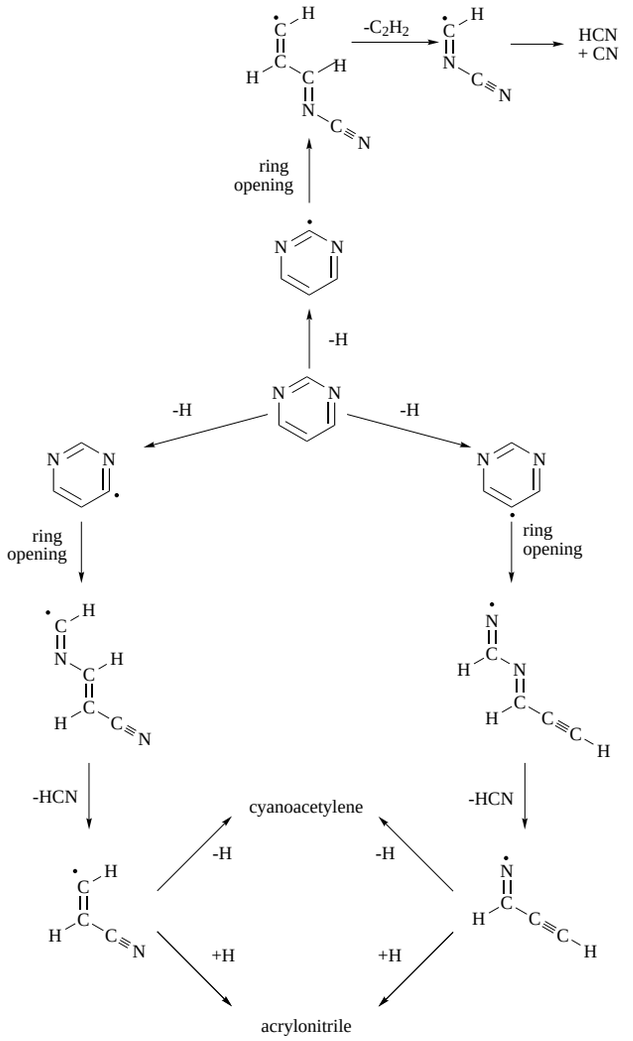

Scheme 3 Low temperature pyrimidine pyrolysis scheme

2-pyrimidyl radicals lead to acetylene and a less stable radical containing two N atoms, which Doughty and Mackie have suggested may lead to highly reactive $^{\bullet}CN$ radicals.[14]

For pyridazine, no products other than HCN and acetylene were observed. This suggests that other mechanisms may be operative here, since the calculations of Table 3 suggest that products such as diacetylene or cyanoacetylene might be expected. However, electron correlation effects render low level calculations extremely unreliable for electrocyclic reactions in aromatic systems. In the light of this, we have carried out calculations at the Møller–Plesset Coupled Cluster (MP2/CC-TZ) level[30] for molecular elimination pathways leading directly to $2HCN + C_2H_2$ or $N_2 + 2C_2H_2$. These calculations suggest that both molecular routes are at least competitive with H atom loss (calculated activation energies are 390 and 360 kJ mol^{-1}, respectively, compared with 440 kJ mol^{-1} for homolytic initiation). On the other hand, the experimental observations suggest that it is the thermodynamically less favoured HCN route which dominates. The results of this and related studies will be reported elsewhere.[30]

Acknowledgements

We thank the University of Auckland for assistance in the purchase of equipment and materials, and for partial financial support of N. R. H. We also acknowledge the invaluable assistance of Dr Noel Renner in the construction of the apparatus, and Sue Glasson for her expertise in obtaining much of the GC–MS data. We also thank Reuben Brown and Peter Schwerdtfeger for communication of the results of *ab initio* calculations for pyridazine.

References

1 D. W. Pershing and J. O. L. Wendt, *Sixteenth Symposium* (*International*) *on Combustion*, The Combustion Institute, Pittsburgh, PA, 1977, p. 389.
2 P. C. Painter and M. M. Coleman, *Fuel*, 1979, **58**, 301.
3 J. Jones, G. B. Bacskay, J. C. Mackie and A. Doughty, *J. Chem. Soc., Faraday Trans.*, 1995, **91**, 1587.
4 C. F. Roth, *Ber.*, 1886, **19**, 360.
5 H. Meyer and A. Hoffmann-Meyer, *J. Prakt. Chem.*, 1921, **102**, 287.
6 S. Ruhemann, *Braunkohle*, 1929, **28**, 749.
7 C. D. Hurd and J. I. Simon, *J. Am. Chem. Soc.*, 1962, **84**, 4519.
8 A. E. Axworthy, V. H. Dayan and G. B. Martin, *Fuel*, 1978, **57**, 29.
9 T. J. Houser, M. E. McCarville and T. Biftu, *Int. J. Chem. Kinet.*, 1980, **12**, 555.
10 R. D. Kern, J. N. Yong, J. H. Kiefer and J. N. Shah, *16th International Symposium on Shock Tubes and Waves*, VCH, Weinheim, 1987, p. 437.
11 H. I. Leidreiter and H. Gg. Wagner, *Z. Phys. Chem.*, 1987, **153**, 99.
12 J. C. Mackie, M. B. Colket and P. F. Nelson, *J. Phys. Chem.*, 1990, **94**, 4099.
13 E. Ikeda and J. C. Mackie, *J. Anal. App. Pyrolys.*, 1995, **34**, 47.
14 A. Doughty and J. C. Mackie, *J. Chem. Soc., Faraday Trans.*, 1994, **90**, 541.
15 A. Doughty, J. C. Mackie and J. M. Palmer, *Twenty-Fifth Symposium* (*International*) *on Combustion*, The Combustion Institute, Pittsburgh, PA, 1994, p. 893.
16 H. Hettema, N. R. Hore, N. D. Renner and D. K. Russell, *Aust. J. Chem.*, 1997, **50**, 363.
17 J. Buckingham and F. Macdonald, *Dictionary of Organic Compounds*, 6th edn., Chapman & Hall, London, 1996.
18 W. M. Shaub and S. H. Bauer, *Int. J. Chem. Kinet.*, 1975, **7**, 509.
19 J. Pola, *Collect. Czech. Chem. Commun.*, 1981, **46**, 2856.
20 D. K. Russell, *Chem. Soc. Rev.*, 1990, **19**, 407; *Coord. Chem. Rev.*, 1992, **112**, 131; *Chem. Vap. Deposition*, 1996, **2**, 223, and references therein.
21 MOLSPEC for Windows, 1993, Laser Photonics Inc., Andover, MA.
22 L. S. Rothman, R. R. Gamache, A. Goldman, L. R. Brown, R. A. Toth, H. M. Pickett, R. L. Poynter, J.-M. Flaud, C. Camy-Peyret, A. Barbe, N. Husson, C. P. Rinsland and M. A. H. Smith, *App. Optics*, 1986, **26**, 4058.
23 N. J. Bristow, B. D. Moore, M. Poliakoff, G. S. Ryott and J. J. Turner, *J. Organomet. Chem.*, 1984, **260**, 180.
24 J. J. P. Stewart, *J. Comp.-Aided. Mol. Design*, 1990, **4**, 1.
25 PC Spartan, Wavefunction Inc., Irvine, CA, 1996.
26 M. H. Brodsky and R. S. Title, *Phys. Rev. Lett.*, 1969, **23**, 581.
27 G. R. Allen and D. K. Russell, unpublished work.
28 *J. Phys. & Chem. Ref. Data*, 1982, **11**, Supplement 2.
29 S. W. Benson, F. R. Cruikshank, D. M. Golden, G. R. Haugen, H. E. O'Neal, A. S. Rodgers, R. Shaw and R. Walsh, *Chem. Rev.*, 1969, **69**, 279.
30 J. R. Brown, N. R. Hore, D. K. Russell and P. A. Schwerdtfeger, unpublished results.

Paper 7/06731C
Received 16*th September* 1997
Accepted 17*th November* 1997